Chemical Science

ROYAL SOCIETY OF CHEMISTRY

EDGE ARTICLE

View Article Online
View Journal | View Issue

Cite this: *Chem. Sci.*, 2026, **17**, 5056

All publication charges for this article have been paid for by the Royal Society of Chemistry

Received 28th October 2025
Accepted 29th December 2025

DOI: 10.1039/d5sc08342g

rsc.li/chemical-science

Near-infrared chemiluminescent probe for real-time monitoring of nitroreductase in tumors

Pan Zhu,†[a] Yu Tang,†[b] Yuanyu Tang,[a] Shaojing Zhao,*[a] Fei Long,[c] Chaoyi Yao,[a] Benhua Wang,[a] Xiangzhi Song,[a] Yi Zhang,*[c] Chaochao Tan*[d] and Minhuan Lan*[a]

Nitroreductase (NTRase) is a hypoxia-associated enzyme that is commonly found in conditions such as inflammatory disorders, myocardial ischemia, and most solid tumors. Therefore, the real-time monitoring of its activity is important for the clinical diagnosis of these conditions. Compared with fluorescence imaging, chemiluminescence (CL) imaging does not require external excitation light, thus exhibiting lower autofluorescence and photobleaching and a higher signal-to-noise ratio (SNR). Herein, we report a near-infrared (NIR) CL probe, namely **NTR-TCN-CL**, for selective and sensitive detection of NTRase. The probe contains a *p*-nitrobenzyl trigger that can be enzymatically reduced by NTRase. The reduction subsequently uncages the CL scaffold, leading to the initiation of chemiexcitation that emits CL signals at ~710 nm. The probe **NTR-TCN-CL** had high specificity and a limit of detection of 0.083 μg mL^{-1} and was successfully employed in imaging of NTRase in 4T1 tumor-bearing mice. The findings demonstrate the potential of the **NTR-TCN-CL** probe in real-time assessment of tumor-associated NTRase activity in the tumor microenvironment and highlight its utilizability as a noninvasive tool for monitoring of the hypoxia-related biomarker.

Introduction

Nitroreductase (NTRase) is a flavin-dependent oxidoreductase that catalyzes the reduction of aromatic nitro groups using reduced nicotinamide cofactors (NADH/NADPH).[1] NTRase activity is elevated in hypoxia-associated pathologies, including certain inflammatory conditions, myocardial ischemia, and most solid tumors.[2,3] Spatiotemporal monitoring of NTRase activity in these conditions is valuable for both diagnosis and therapeutic guidance. Numerous optical strategies have been developed for NTRase detection.[4–6] Fluorescence (FL) imaging offers high sensitivity.[7,8] However, it requires external excitation, which restricts tissue penetration and induces photobleaching and autofluorescence.[9–11] Bioluminescence (BL) probes diminish the need for external light and generate deep-tissue signals through luciferin-luciferase reactions.[12,13] Li *et al.* reported a luciferin-based BL probe for NTRase detection that emits BL signals at 560 nm and has a limit of detection (LOD) of 0.001 μg mL^{-1}. Chan and colleagues later developed a near-infrared (NIR) BL probe, BL660-NTR (λ_{em} = 660 nm), by conjugating a luciferin analog BL660 with isopropyl *p*-nitrobenzyl alcohol. They reported that the isopropyl group enhances the stability of the probe against enzymatic hydrolysis (Scheme 1a). However, these probes rely on luciferase expression (*via* transgenesis or delivery), thus, their applicability in native physiological contexts is limited.[14–17] These limitations motivate the development of chemiluminescence (CL) probes that can overcome such drawbacks and improve the signal-to-noise ratio (SNR) *in vivo*.[18,19]

Schaap's dioxetane scaffolds have recently been used as activatable CL probes due to their rapid chemiexcitation high brightness, structural tunability, and activatability.[20–25] Structural modifications of Schaap's dioxetane have yielded probes that emit CL upon activation by NTRase (Scheme 1b).[26–28] Lippert *et al.* reported HyCL-4-AM, a dioxetane-based probe bearing a *p*-nitrobenzyl group that generates green CL at ~540 nm upon enzymatic reduction.[27] Zhang *et al.* improved the water solubility of the probe by incorporating an acrylic acid moiety into the dioxetane scaffold, yielding CL-NTR that can accurately detect NTRase with a LOD of 0.947 ng mL^{-1} under aqueous conditions.[26] Pu *et al.* further advanced the field by introducing a strong electron-accepting unit (*N*-ethylrhodamine-methylene-4*H*-benzopyran) to construct HEDPN, a NIR-emitting probe with

[a]*College of Chemistry and Chemical Engineering, Central South University, Changsha, 410083, P. R. China. E-mail: 31180030@csu.edu.cn; minhuanlan@csu.edu.cn*

[b]*Gastroenterology and Urology Department* II, *The Affiliated Cancer Hospital of Xiangya School of Medicine, Central South University/Hunan Cancer Hospital, Changsha, 410013, P. R. China*

[c]*Department of Gastrointestinal Surgery, The Third Xiangya Hospital of Central South University, Changsha, 410013, P. R. China. E-mail: yzhangxy3@csu.edu.cn*

[d]*Department of Clinical Laboratory, The First Affiliated Hospital of Hunan Normal University (Hunan Provincial People's Hospital), Changsha, 410005, P. R. China. E-mail: tchchwolf@163.com*

† P. Z. and Y. T. contributed to this work equally.

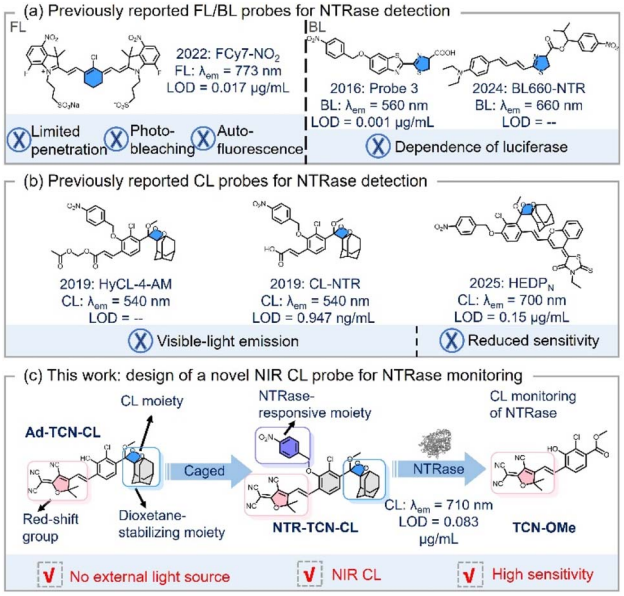

Scheme 1 (a) Representative previously reported FL/BL probes and (b) CL imaging probes for NTRase detection. (c) This work: design of a NIR CL probe for NTRase monitoring.

a maximal CL at ~700 nm and a LOD of 0.15 μg mL^{-1}.[28] These examples demonstrate the potential applications of Schaap's dioxetane in CL probes. However, most reported CL probes suffer from either visible-light emission, which limits imaging depth, or insufficient sensitivity for accurate NTRase monitoring. Thus, there is an urgent need for high-performance CL sensors for accurate, deep-tissue imaging of NTRase activity *in vivo*.

Here, we report a novel NTRase-responsive probe **NTR-TCN-CL**. The probe was constructed from a novel NIR dioxetane scaffold, **Ad-TCN-CL**, which was prepared by introducing the strongly electron-withdrawing acceptor 2-(3-cyano-4,5,5-trimethylfuran-2(5*H*)-ylidene) malononitrile (to achieve red-shifted emission). **Ad-TCN-CL** was then capped with a *p*-nitrobenzyl trigger, resulting in **NTR-TCN-CL**. The probe showed high specificity for NTRase in aqueous media, exhibited CL emission at ~710 nm, and had a LOD of 0.083 μg mL^{-1} (Scheme 1c). *In vivo* imaging in tumor models showed that **NTR-TCN-CL** could be activated by both exogenous and endogenous NTRase. These results demonstrate that **NTR-TCN-CL** is a promising NIR CL probe for specific and sensitive assessment of tumor-associated NTRase activity in physiological environments.

Results and discussion

Design and synthesis of the NIR CL probe Ad-TCN-CL

To elucidate the CL signal generation mechanism of **NTR-TCN-CL**, we synthesized an uncaged CL probe called **Ad-TCN-CL** by conjugating an electron-withdrawing group, 2-(3-cyano-4,5,5-trimethylfuran-2(5*H*)-ylidene) malononitrile (TCN), with Schaap's dioxetane (Fig. 1a). All compounds were characterized by HRMS and ^{1}H and ^{13}C NMR (Fig. S1–S10). **Ad-TCN-CL** was converted to a phenoxide ion in slightly basic PBS. Then, 2-adamantanone was eliminated through a chemically initiated electron exchange luminescence (CIEEL) process, accompanied by the generation of the excited state of **TCN-OMe**, **[TCN-OMe]***.

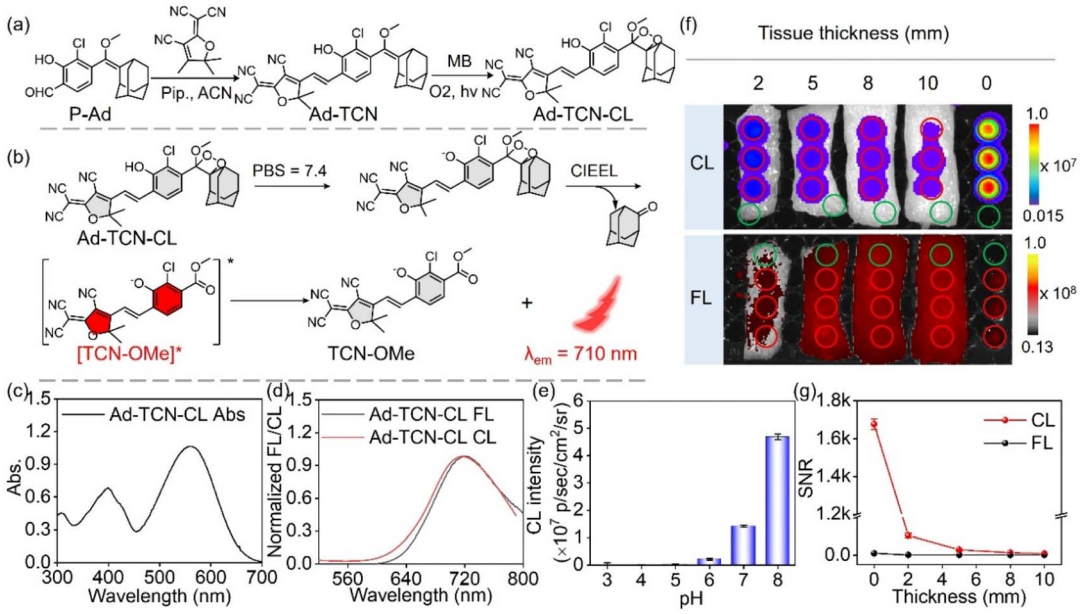

Fig. 1 (a) Synthesis route of the CL probe **Ad-TCN-CL**. (b) Schematic illustration of CL generation by **Ad-TCN-CL** in PBS. (c) Absorption and (d) FL (λ_{ex} = 550 nm)/CL spectra of **Ad-TCN-CL** in PBS. (e) Effect of pH on CL intensity of **Ad-TCN-CL** (50 μM) in PBS. (f) CL imaging of **Ad-TCN-CL** (100 μM) and FL imaging (λ_{ex} = 540 nm and λ_{em} = 710 nm) of **Ad-TCN** (100 μM) in PBS under chicken tissues of varying thicknesses. Green circles indicate the background region chosen and red circles indicate the CL/FL region chosen. (g) Quantification of SNR in (f). Unless otherwise stated, the pH of PBS was 7.4.

The CL emission results from the radiative transition of **[TCN-OMe]*** to its ground state (Fig. 1b). The absorption and fluorescence spectra of **Ad-TCN-CL** in PBS were first investigated by using UV-2600 and RF-6000 spectrometers. Two absorption bands appeared at 400 nm and 550 nm (Fig. 1c). A strong NIR FL emission was observed at 720 nm (Fig. 1d). The CL properties of **Ad-TCN-CL** in PBS were subsequently examined using an IVIS imaging system. The CL intensity of **Ad-TCN-CL** was measured across different emission channels (520, 570, 620, 670, 710, and 790 nm). As shown in Fig. 1d, **Ad-TCN-CL** exhibited the strongest luminescence at ~710 nm, consistent with the characteristic FL emission.

To further investigate the decomposition process responsible for CL emission, the compound **TCN-OMe** (Scheme S1) was synthesized independently. The absorption and FL spectra of **TCN-OMe** closely resembled those of **Ad-TCN-CL** under basic conditions (Fig. S11a and b). Moreover, **TCN-OMe** exhibited an absorption peak at 550 nm and its maximum emission appeared at 720 nm as pH increased, and the pK_a of **TCN-OMe** was calculated to be 5.6 (Fig. S11c). To rationalize the observed absorption and emission wavelengths, density functional theory (DFT) calculations were performed at the PBE0/def2-TZVP-SMD (water) level. The electron density distributions of the highest occupied molecular orbitals (HOMO) and lowest unoccupied molecular orbitals (LUMO) of protonated and deprotonated **TCN-OMe** are shown in Fig. S12. In protonated **TCN-OMe**, the electrons in the HOMO and LUMO were predominantly delocalized across the molecular skeleton. Upon deprotonation, the HOMO localized primarily on the benzoate unit, and the contribution from the TCN moiety was reduced. By contrast, the LUMO exhibited increased electron density on the TCN group, indicative of a pronounced charge transfer. The calculated HOMO–LUMO energy gaps for the protonated and deprotonated forms were 3.42 eV and 2.82 eV, respectively, consistent with the observed red shift in absorption and emission wavelengths. These findings indicate that the NIR luminescence of **Ad-TCN-CL** in PBS originates from a pronounced intramolecular charge transfer process,[29] facilitated by the synergistic interaction between the strongly electron-withdrawing tricyanofuran (TCN) moiety and the electron-donating phenoxide. Investigation into pH-dependent CL demonstrated that alkaline conditions significantly enhanced the initiation efficiency of CL in **Ad-TCN-CL** (Fig. 1e and S13). These results strongly support the proposed mechanism by which **Ad-TCN-CL** generates CL emission under basic conditions.

Tissue-penetrating capacity of chemiluminescence generated by Ad-TCN-CL

To evaluate tissue-penetrating capacity, **Ad-TCN-CL** or **Ad-TCN** was overlaid with chicken tissues of varying thicknesses (2, 5, 8, and 10 mm), and their CL or FL images were recorded. CL imaging could detect luminescent signals through 10 mm of chicken breast tissue. In contrast, FL imaging produced detectable signals only through 5 mm of tissue. The SNR of CL imaging was 7-fold higher than that of FL imaging with 10 mm tissue. These results confirm that the CL method not only generates high-SNR signals but also demonstrates excellent performance for deep-tissue imaging (Fig. 1f and g).

Design and synthesis of the NTRase-activated probe NTR-TCN-CL

Building on the favorable CL performance of **Ad-TCN-CL**, we incorporated a *p*-nitrobenzyl group into **Ad-TCN-CL** to construct an NTRase-activated NIR CL probe. The synthetic route of **NTR-TCN-CL** is depicted in Fig. 2a, and the confirmation of its structure by HRMS and ^{1}H and ^{13}C NMR is presented in Fig. S14–S22. The mechanism involves NTRase-mediated reduction of the nitro group on **NTR-TCN-CL** to yield an aryl imine anion, followed by intramolecular 1,4-elimination to generate deprotonated **Ad-TCN-CL**, which then undergoes a CIEEL process to release luminescence, consistent with the mechanism of **Ad-TCN-CL**. The response of **NTR-TCN-CL** to

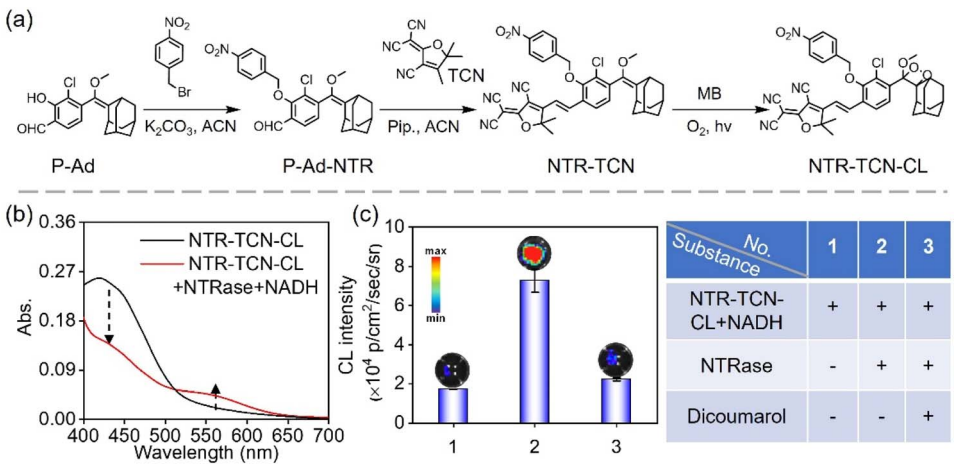

Fig. 2 (a) Synthesis route of **NTR-TCN-CL**. (b) Absorption spectra of **NTR-TCN-CL** (15 μM) in the presence and absence of NTRase (10 μg mL^{-1}) in PBS at 37 °C (NADH: 500 μM). (c) CL intensity of **NTR-TCN-CL** (25 μM) with NTRase in the presence and absence of dicoumarol (NADH: 500 μM, dicoumarol: 100 μM).

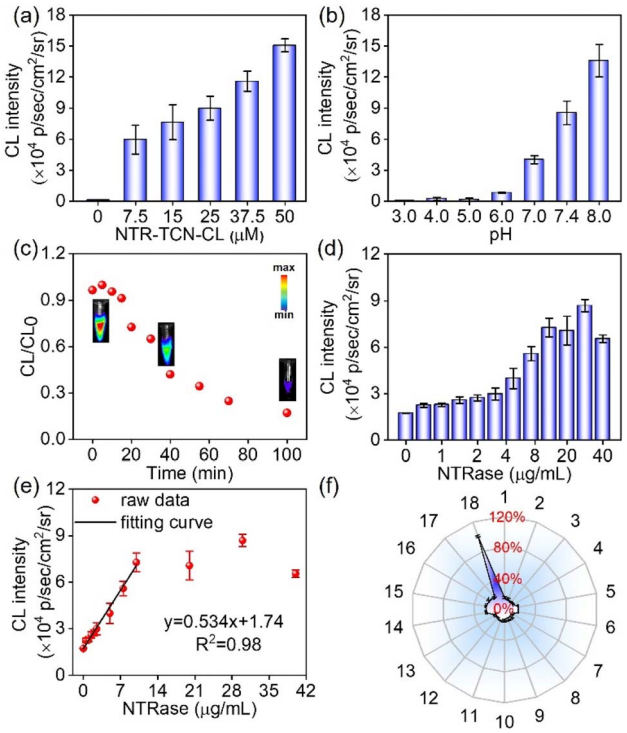

Fig. 3 (a) CL intensity of **NTR-TCN-CL** at varying concentrations in the presence of NTRase (10 μg mL^{-1}). (b) Effect of pH on the CL intensity of **NTR-TCN-CL** (25 μM). (c) CL kinetics and images (inset) of **NTR-TCN-CL** (25 μM) following the addition of NTRase (10 μg mL^{-1}). (d) CL intensity of **NTR-TCN-CL** upon addition of NTRase at different concentrations. (e) Linear relationship between CL intensity of **NTR-TCN-CL** and NTRase concentration in the range of 0–10 μg mL^{-1}. (f) Selectivity of **NTR-TCN-CL** (25 μM) toward various analytes (1: histidine, 2: lysine, 3: alanine, 4: valine, 5: serine, 6: glycine, 7: aspartic acid, 8: glutathione, 9: KCl, 10: $NaHCO_3$, 11: Na_2SO_3, 12: $FeSO_4$, 13: L-ascorbic acid, 14: NADH, 15: AzoRase, 16: HNQO1, 17: LDA, and 18: NTRase, 500 μM for 1–14; 10 μg mL^{-1} for 15–18). All measurements were carried out in PBS at 37 °C.

NTRase was then evaluated in PBS (Fig. 2b). Upon exposure to NTRase, the absorption at 400 nm of **NTR-TCN-CL** decreased, and a new absorption peak at 550 nm appeared. As anticipated, in the presence of NTRase, **NTR-TCN-CL** elicited intense CL emission. In contrast, NTRase treated with dicoumarol, a known inhibitor of NTRase, markedly attenuated the luminescent signal (Fig. 2c). These results indicate that **NTR-TCN-CL** responds selectively to NTRase, producing robust CL emission.

Response of NTR-TCN-CL to NTRase *in vitro*

CL intensity increased with increasing concentrations of **NTR-TCN-CL** (Fig. 3a and S23). The CL intensity of **NTR-TCN-CL** upon treatment with NTRase was subsequently evaluated under different pH conditions. As illustrated in Fig. 3b and S24, CL intensity gradually increased with increasing pH from 3 to 8. A pronounced CL signal was observed near physiological pH (7.4). Based on these findings, 25 μM **NTR-TCN-CL** at pH 7.4 was selected as the optimal condition for subsequent detection experiments. Luminescence kinetics of **NTR-TCN-CL** revealed a typical CL kinetic profile (Fig. 3c). The profile showed a rapid onset, reaching maximum intensity within ~5 min, followed by a gradual decay of CL with a half-life of ~35 min. Additionally, the CL response was evaluated across a range of enzyme concentrations. The results verify that the system exhibits a wide linear dynamic range from 0 to 10 μg mL^{-1}, with a calculated LOD of 0.083 μg mL^{-1}. The system's sensitivity is further evidenced by a clearly measurable signal (2.25×10^4 p per sec per cm^2 per sr) at the lowest tested concentration of 0.5 μg mL^{-1}, corresponding to a 1.3-fold increase over the NTRase-free control. At concentrations exceeding 20 μg mL^{-1}, the CL intensity reached a plateau, indicating the system's upper limit for quantitative measurement. These findings demonstrate the suitability of **NTR-TCN-CL** for the sensitive quantification of NTRase (Fig. 3d and e, and S25).

The specificity of **NTR-TCN-CL** to NTRase was examined. **NTR-TCN-CL** solutions were incubated with various potential-

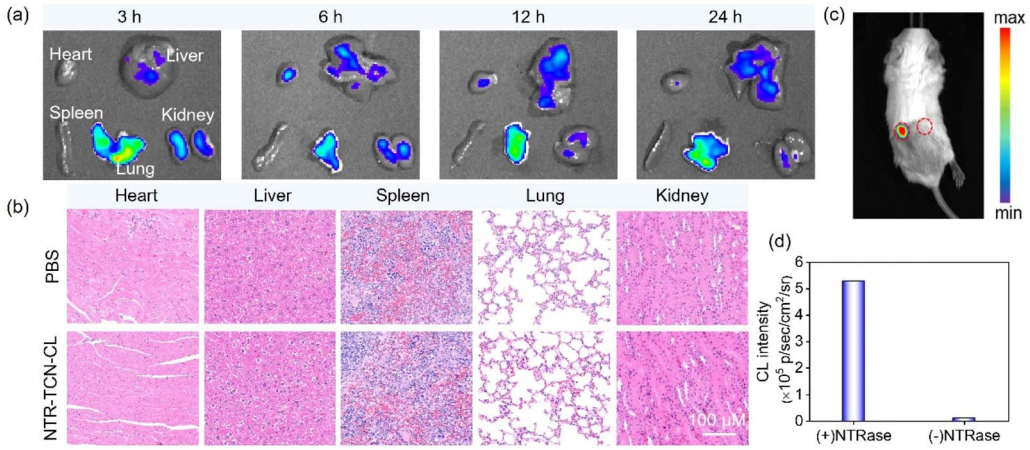

Fig. 4 (a) Fluorescence images (λ_{ex} = 420 nm and λ_{em} = 620 nm) of *ex vivo* organs at 3, 6, 12 and 24 h after tail vein injection of **NTR-TCN-CL** (100 μM). (b) H&E staining of major organs of the mice after treatment of PBS or **NTR-TCN-CL**. (c) CL images of a Balb/c mouse. The left dorsal site was injected with **NTR-TCN-CL** (100 μM) along with NTRase (20 μg mL^{-1}) + NADH (500 μM), whereas the right site received only **NTR-TCN-CL** (100 μM). (d) Quantification of the CL intensity from (c).

interfering substances, including histidine, lysine, alanine, valine, serine, glycine, aspartic acid, glutathione, KCl, $NaHCO_3$, Na_2SO_3, $FeSO_4$, L-ascorbic acid, NADH, azoreductase (AzoRase), human NAD(P)H quinone oxidoreductase 1 (HNQO1), lactate dehydrogenase (LDH) and NTRase, and CL signals were measured using the IVIS system. As depicted in Fig. 3f and S26, the CL intensity was significantly enhanced in the presence of NTRase compared to all other tested substances. To assess the stability of **NTR-TCN-CL**, we monitored its absorption spectra over a 5 day period at 4 °C. As shown in Fig. S27, the spectra of **NTR-TCN-CL** in PBS exhibited minimal variation, indicating good chemical stability.

Biosafety evaluation and *in vivo* CL imaging of exogenous NTRase for NTR-TCN-CL

To evaluate the potential biosafety during imaging of **NTR-TCN-CL** *in vivo*, first, cellular uptake of **NTR-TCN-CL** was confirmed using its FL under 405 nm excitation. As shown in Fig. S28, red FL signals were observed after 15 min of incubation, suggesting that **NTR-TCN-CL** can be rapidly uptaken by 4T1 cells. We further assessed the biodistribution of **NTR-TCN-CL** by harvesting major organs (heart, liver, spleen, lungs, and kidneys) at 3, 6, 12, and 24 h after tail vein injection and performing *ex vivo* fluorescence imaging (Fig. 4a and S29). The results revealed initial accumulation of **NTR-TCN-CL** mainly in the lungs at 3 h, followed by a gradual decrease in pulmonary fluorescence over time. In parallel, a progressive increase in fluorescence was detected in the liver, while renal signals showed a consistent decline. Only minimal fluorescence was observed in the heart and spleen throughout the experimental period. These data suggest that **NTR-TCN-CL** undergoes systemic circulation and is subsequently metabolized through both hepatic and renal pathways.

In addition, the cytotoxicity of **NTR-TCN-CL** and its enzymatically decomposed product **TCN-OMe** was evaluated using MTT assays (Fig. S30). After 24 h of treatment with 50 μM of either the probe or **TCN-OMe**, over 80% viability was maintained in 4T1 cells, indicating negligible cytotoxicity. Supplementary hematoxylin and eosin (H&E) staining and hemolysis assays further supported the biosafety profile of the compounds. As shown in Fig. 4b, S31, and S32, H&E-stained tissue slices from major organs of mice treated with **NTR-TCN-CL** or **TCN-OMe** *via* tail vein injection exhibited no signs of apparent toxicity or pathological lesions. Moreover, both compounds demonstrated negligible hemolytic activity *in vitro*, with a hemolysis rate below 3%. Together, these results confirm the high biocompatibility of **NTR-TCN-CL** and support its safety for further biological applications. The potential of **NTR-TCN-CL** to detect NTRase *in vivo* through CL imaging was subsequently investigated. **NTR-TCN-CL** with or without NTRase + NADH was subcutaneously injected into the dorsal region of healthy Balb/c mice. CL images were subsequently acquired. CL imaging showed substantial enhancement in **NTR-TCN-CL** signals in the presence of NTRase + NADH. The CL intensity on the left dorsal region was 50-fold higher than that on the right (Fig. 4c and d). These results suggest that **NTR-TCN-CL** can serve as an effective *in vivo* luminescence agent.

In vivo CL imaging of endogenous NTRase using NTR-TCN-CL

Real-time imaging has revolutionized the field of medical diagnostics by offering a non-invasive and precise approach for disease diagnosis. Encouraged by the high sensitivity, selectivity, and long half-life of **NTR-TCN-CL**, we investigated its ability to visualize NTRase activity in tumors. First, a subcutaneous tumor model was established in mice using 4T1 cells. The 4T1 tumor-bearing mice were subsequently divided into two groups: "PBS" and "$CoCl_2$". These groups received treatments of PBS and $CoCl_2$, respectively. The $CoCl_2$ treatment induced moderate hypoxia, as a result of Co^{2+} binding to the hypoxia-inducible factor (HIF).[30] Two hours after PBS or $CoCl_2$ treatment, **NTR-TCN-CL** was administered intratumorally, and imaging was performed using the IVIS system (Fig. 5a). As shown in Fig. 5b and c, in the "PBS" group, the CL intensity of

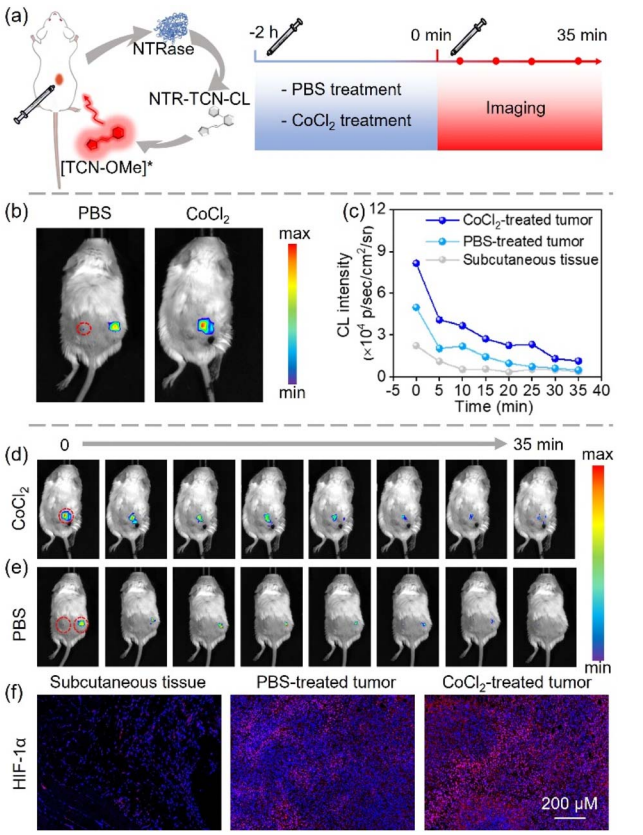

Fig. 5 (a) Schematic illustration summarizing the procedures for *in vivo* imaging of endogenous NTRase using **NTR-TCN-CL** (100 μM) and the timeline for treatment and imaging. (b) CL images of 4T1 tumor-bearing mice treated with $CoCl_2$ (right) or PBS (left). The red circle indicates the CL signal of **NTR-TCN-CL** in the subcutaneous tissue. (c) Quantification of the time-dependent CL intensity from (d) and (e). CL images of 4T1-bearing mouse treated with (d) $CoCl_2$ (the red circle indicates the tumor site) and (e) PBS (the left red circle indicates the tumor site, and the right red circle indicates the subcutaneous tissue) recorded at 5 min intervals. (f) Immunofluorescence images of HIF-1α in the normal tissue or tumor slices from different treatment groups.

NTR-TCN-CL in the tumor was about 2-fold higher than that in normal subcutaneous tissue. In the "$CoCl_2$" group, the CL intensity was 4-fold higher than that in the normal tissue. Immunohistochemical analysis confirmed a significant upregulation of HIF-1α in tumor tissues from $CoCl_2$-treated mice compared to the PBS-treated control and normal tissue (Fig. 5f). This finding indicates that $CoCl_2$ successfully induced a hypoxic tumor microenvironment, which in turn enhanced NTRase activity. In addition, *in vivo* CL kinetics were studied by capturing luminescence signals at 5 min intervals. Dynamic imaging revealed that the "$CoCl_2$" group could maintain luminescence for over 35 min, in contrast to the "PBS" group (Fig. 5c–e). The above results demonstrate that **NTR-TCN-CL** is a potent tool for real-time monitoring of NTRase activity in tumors.

Conclusions

In summary, a novel NIR chemiluminophore, **Ad-TCN-CL**, was developed using Schaap's dioxetane scaffold. Under basic conditions, **Ad-TCN-CL** emitted CL signals at ~710 nm. The CL generated by **Ad-TCN-CL** had superior tissue penetration and a high SNR ratio. The NTRase-activated CL probe, **NTR-TCN-CL**, was constructed by capping the hydroxyl group of **Ad-TCN-CL** with a *p*-nitrobenzyl group. The probe showed high selectivity and sensitivity for NTRase (LOD = 0.083 μg mL^{-1}). *In vivo* experiments revealed that **NTR-TCN-CL** could be activated in tumors. **NTR-TCN-CL** generated CL signals about 4-fold stronger in the tumor of mice treated with $CoCl_2$ than in subcutaneous tissue. The CL signal persisted for up to 35 min. Overall, this work presents an effective strategy for real-time visual monitoring of NTRase activity in tumors.

Ethical statement

All animal procedures were performed in accordance with the Guidelines for Care and Use of Laboratory Animals of Hunan Normal University (China) and approved by the Animal Ethics Committee of Hunan Normal University (No. D2024026).

Author contributions

P. Z., S. Z., Y. Z., C. T., and M. L. conceived the ideas and designed the studies. P. Z. carried out the synthesis, photophysical and chemical studies. P. Z. and Y. T. designed and performed the studies for *in vivo* CL imaging of NTRase. P. Z., Y. T. and M. L. wrote the manuscript. All authors reviewed and approved the final version of the manuscript.

Conflicts of interest

There are no conflicts to declare.

Data availability

The authors confirm that the data supporting the findings of this study are available within the article and its supplementary information (SI). Supplementary information: experimental protocols, compound characterization, FL spectra, CL images and biochemical experiments. See DOI: https://doi.org/10.1039/d5sc08342g.

Acknowledgements

This work was supported by the National Natural Science Foundation of China (No. 62375289, 62175262), the Hunan Provincial Health and Medical Research Project (No. 20256892), the Science and Technology Innovation Team Project of Hunan Provincial People's Hospital (KCT202402) and Hunan University of Traditional Chinese Medicine's Discipline Construction Project of "Exposing the List and Taking the Lead" (22JBZ037). This work was carried out in part using hardware and/or software provided by the High-Performance Computing Center of Central South University.

References

1 X. Li, J. Ai, Y. Zhang, F. Huo and C. Yin, *Nano Today*, 2025, **63**, 102768.
2 N. Zhang, T. Li, P. Zhong, T. Fu, L. Li, M. Peng, Y. Wang, Y. Lu and M. Yao, *J. Med. Chem.*, 2025, **68**, 14981–14994.
3 S. Sarkar, A. Shil, Y. W. Jun, Y. J. Yang, R. Cheng, W. Wu, X. Li, Q. Hu and K. H. Ahn, *Adv. Sci.*, 2025, **12**, e08689.
4 Y. Tian, L. Wang, R. Chen, Y. Miao, Y. Liu, W. Huang, L. Fang, S. Liu, J. Luo, X. Sun, Y. Zhang and D. Ye, *Angew. Chem., Int. Ed.*, 2025, **64**, e202500645.
5 S. Zhang, X. Liu, B. P. Jiang, S. C. Ji, H. Chen and X. C. Shen, *Anal. Chem.*, 2025, **97**, 13637–13645.
6 L. Lei, K. Li, Y. F. Tang, Y. H. Liu, S. X. Wu, G. L. Huang, H. C. Lin, Z. Zhang, K. Hong, W. M. Xu, X. Q. Yu and K. K. Yu, *ACS Sens.*, 2025, **10**, 4733–4743.
7 S. Chen, L. Xiao, Y. Li, M. Qiu, Y. Yuan, R. Zhou, C. Li, L. Zhang, Z. X. Jiang, M. Liu and X. Zhou, *Angew. Chem., Int. Ed.*, 2022, **61**, e202213495.
8 Y. Dong, Y. Zou, X. Jia, L. Yin, W. He, X. Luo, X. Qian and Y. Yang, *Smart Mol.*, 2023, **1**, e20230001.
9 Y. Lin, J. Huang, J. Liu, M. Xu, C. Xu and K. Pu, *J. Am. Chem. Soc.*, 2025, **147**, 2597–2606.
10 S. Huang, S. Bai, T. Luo, F. Zheng, D. Fan, Y. J. Zhou, F. Chen and W. Zeng, *Adv. Funct. Mater.*, 2024, **34**, 2409292.
11 L. Yang, M. Zhao, W. Chen, J. Zhu, W. Xu, Q. Li, K. Pu and Q. Miao, *Angew. Chem., Int. Ed.*, 2024, **63**, e202313117.
12 P. Feng, H. Zhang, Q. Deng, W. Liu, L. Yang, G. Li, G. Chen, L. Du, B. Ke and M. Li, *Anal. Chem.*, 2016, **88**, 5610–5614.
13 A. K Yadav, Z. Zhao, Y. Weng, S. H Gardner, C. J Brady, O. Peguero and J. Chan, *J. Am. Chem. Soc.*, 2023, **145**, 1460–1469.
14 S. L. O'Brien, E. Tripp, N. Barki, E. G. Blondel-Tepaz, A. Boufersaoui, J. Roberts, J. A. Pike, J. Correia, T. Miljus, M. Bouvier, D. A. Tennant, B. D. Hudson, Z. Gerhart-Hines, G. Milligan, T. W. Schwartz and D. Calebiro, *Nat. Chem. Biol.*, 2026, **22**, 109–119.
15 A. J. Syed and J. C. Anderson, *Chem. Soc. Rev.*, 2021, **50**, 5668–5705.

16 L. Wang, Y. Liu, J. Sun, J. Su, J. Feng, L. Miao, W. Zhao, H. Zhang and K. Liu, *ACS Nano*, 2025, **19**, 26791–26804.
17 B. Zhou, F. Wu, B. Zheng, T. Hu, X. Qiu, K. Yang and H. Xiong, *Chin. Chem. Lett.*, 2025, DOI: 10.1016/j.cclet.2025.111835.
18 Y. Zhang, T. Y. He, X. He, S. Huang and Q. X. Wang, *CCS Chem.*, 2025, **7**, 2532–2536.
19 R. Tannous, T. Kopp and D. Shabat, *JACS Au*, 2025, **5**, 2871–2883.
20 R. Tannous, O. Shelef, S. Gutkin, M. David, T. Leirikh, L. Ge, Q. Jaber, Q. Zhou, P. Ma, M. Fridman, U. Spitz, K. N. Houk and D. Shabat, *ACS Cent. Sci.*, 2024, **10**, 28–42.
21 M. David, T. Leirikh, N. Naama, T. Kopp and D. Shabat, *Angew. Chem., Int. Ed.*, 2025, **64**, e202515674.
22 K. Liao, L. Zhang, J. Jiang, F. Wang and T. Peng, *Angew. Chem., Int. Ed.*, 2025, **64**, e202514236.
23 O. Shelef, S. Gutkin, D. Feder, A. Ben-Bassat, M. Mandelboim, Y. Haitin, N. Ben-Tal, E. Bacharachc and D. Shabat, *Chem. Sci.*, 2022, **13**, 12348–12357.
24 J. Yang, Y. Yang, H. Wang, S. H. Liang and C. Ran, *Angew. Chem., Int. Ed.*, 2025, **64**, e202507174.
25 Z. Chen, Q. Li, Y. Wu, J. Liu, L. Liu, L. Su, R. Wu and J. Song, *Nat. Commun.*, 2025, **16**, 238.
26 J. Sun, Z. Hu, R. Wang, S. Zhang and X. Zhang, *Anal. Chem.*, 2019, **91**, 1384–1390.
27 L. S. Ryan, J. Gerberich, J. Cao, W. An, B. A. Jenkins, R. P. Mason and A. R. Lippert, *ACS Sens.*, 2019, **4**, 1391–1398.
28 J. Huang, J. Liu, J. Wu, M. Xu, Y. Lin and K. Pu, *Angew. Chem., Int. Ed.*, 2025, **64**, e202421962.
29 L. Du, X. Li, B. Li, R. Ding, Q. Zhang, Y. Guo, Q. Zhang, Y. Wang, J. Chen, X. Zhou, Z. Qian and J. Zhou, *Anal. Chem.*, 2025, **97**, 16896–16905.
30 Y. Jiao, L. Zhang, X. Gao, W. Si and C. Dua, *Angew. Chem., Int. Ed.*, 2020, **59**, 6021–6027.